Noname manuscript No.
(will be inserted by the editor)

Flow over a rounded backward-facing step, comparing a z-coordinate model and a σ-coordinate model

Kristin Rygg · Guttorm Alendal · Peter Mosby Haugan

Received: date / Accepted: date

Abstract Homogeneous, non-rotating flow over a backward-facing rounded step is simulated using the 2D vertical (2DV) version of two general circulation models, a z-coordinate model, the Massachusetts Institute of Technology general circulation model (MITgcm), and a σ-coordinate model, the Bergen Ocean Model (BOM). The backward-facing step is a well known testcase since it is geometrically simple, but still embodies important turbulence characteristics such as separation point, reattachment length, and recirculation of the flow. The study includes Reynolds numbers, based on the vertical eddy viscosity ranging from $2{\cdot}10^2$ to $2{\cdot}10^6$. The results correspond with previous published results with a relatively stationary separation point and a fluctuating reattachment length due to downslope propagating eddies released from the reattachment zone for Reynolds numbers higher than or equal to $2 \cdot 10^4$. For Reynolds number within the laminar regime the flow is stationary. The discrepancies between the models increase for enhancing Reynolds number, where the σ-coordinate model experiences reduction in the eddy sizes with increasing resolution and Reynolds numbers in correspondence with published experiments, while the size of the eddies are independent of Reynolds number using the MITgcm. The reattachment zone is shifted upstream in the σ-coordinate model compared to in the z-coordinate model for high Reynolds number ($\geq 2 \cdot 10^5$). The z-coordinate model gives better convergence of the

K. Rygg
UniComputing, Høyteknologisenteret,Thormøhlensgate 55,N-5008 Bergen, Norway.
Tel.: 0047-55584075
Fax: 0047-55584295
E-mail: kristin.rygg@uni.no

G. Alendal
Department of Mathematics, University of Bergen, Johannes Brunsgate 12, 5008 Bergen, Norway.
UniComputing, Høyteknologisenteret,Thormøhlensgate 55,N-5008 Bergen, Norway.

P. M. Haugan
Geophysical Institute, University of Bergen, Allégaten 70, 5007 Bergen, Norway.

separation point and reattachment length than BOM due to mixing generated by the staircase topography.

Keywords Backward facing step · separation · reattachment · MITgcm · BOM

1 Introduction

Modeling the ocean is a huge challenge since the ocean consists of a wide range of processes, with active scales ranging from Rossby waves with a length scale of 10^5 m (Colling, 1989) to molecular processes as gas exchange with a length scale of $4{\cdot}10^{-5}$ m (Broecker and Peng, 1982). Numerical models can only represent phenomena larger than twice the grid size (Haidvogel and Beckmann, 1998). Hence modeling small scales requires high computational costs, and assumptions related to sub-scale modeling need to be done.

The resolution in ocean models is in general too coarse to resolve small scale topography, and topographic effects are therefore often parameterized. Rough topography leads to enhanced mixing (Poltzin et al., 1997; Ledwell et al., 1998). A good estimate of the bottom current is important for studying local bottom processes as sediment transport and transport of pollutants. Examples of such studies are food access for cold-water corals (Thiem et al., 2006, 2008), and transport of chemical transports in the bottom layer; as CO_2 injected directly into the water column and leakages of CO_2 from reservoirs below the bottom of the ocean (Fer and Haugan, 2003; Haugan and Alendal, 2005; House et al., 2006; Kano et al., 2009). The bottom boundary layer is also important for studying how the local meiofauna is affected by increased concentrations of chemical compounds (Auerbach et al., 1997).

The choice of vertical coordinate system leads to different benefits and disadvantages related to discretization of the governing equations. Terrain-following σ-coordinates accurately describe the bottom topography and the kinematic boundary condition, and also allows for a free moving surface. When the bottom topography is transformed into a Cartesian grid, truncation errors are introduced as the bottom is represented by a staircase topography (Kantha and Claysson, 2000). This error affects the overall circulation (Greenberg et al., 2007). The effect of the truncation error at the bottom can be reduced by using shaved cells (Adcroft et al., 1997) or by special turbulence schemes (Greenberg et al., 2007).

In cases with large depth variations, z-coordinate models strive with a large number of inactive cells and difficulties to achieve sufficient resolution of the bottom boundary layer (Kantha and Claysson, 2000). Using a σ-coordinate models this is a problem which essentially can be solved by introducing enough σ-layers near the bottom (Haidvogel and Beckmann, 1998).

The horizontal pressure term is important for the momentum balance. In a z-coordinate model the horizontal pressure term can be calculated accurately (Kantha and Claysson, 2000). The opposite is the case for the σ-coordinate models, where the horizontal pressure error can be large in regions with rapid

topographic changes (Berntsen, 2002). Several options have been suggested to avoid and reduce this problem (Gary, 1973; McCalpin, 1994; Stelling and van Kester, 1994; Mellor et al., 1998; Thiem and Berntsen, 2006), but at present there is no universal method to solve the internal pressure error problem in σ-coordinates.

Diffusion is added to the model to ensure numerical stability. The mixing in the ocean mainly occur over pycnoclines, but is normally implemented along the coordinate surfaces of the model, leading to problems with spurious diapycnal diffusion for both z-coordinate models and σ-coordinate models (Kantha and Claysson, 2000). In σ-coordinate models the horizontal diffusion is suggested set to 0 to avoid spurious mixing related to sharp topographies (Mellor and Blumberg, 1985).

One of the most common assumptions in ocean modeling is the hydrostatic assumption. The hydrostatic assumption is valid on a global scale, for large wind-driven gyres of scales of 1000s of kilometers, and geostrophic eddies of range 10-100 kilometers (Marshall et al., 1997). However the hydrostatic assumption begins to break down as the horizontal length scale becomes of the same range as the vertical scale (Marshall et al., 1997). Marshall et al. (1997) presented the non-hydrostatic parameter, $n = \frac{\gamma^2}{Ri}$ as a measure of when non-hydrostatic processes should be included. The non-hydrostatic pressure should be included when $n << 1$. Here γ represents L_v/L_h the ratio of the vertical scales over the horizontal scales, and Ri the Richardson number. Including the non-hydrostatic pressure leads to an elliptic equation for the non-hydrostatic pressure (Keilegavlen and Berntsen, 2009), and higher computational costs. The non-hydrostatic pressure should therefore only be included when such processes are important, and additionally the resolution is sufficient to resolve the non-hydrostatic processes. Berntsen et al. (2009) found through simulations of flow over a sill that for horizontal grid sizes of 50 to 100 meters the non-hydrostatic pressure effects were small, but for smaller grid sizes the non-hydrostatic correction term clearly affected the solution. In their simulations the vertical grid sizes ranged between 0.5 meter to 1 meter depending on the local depth (Berntsen et al., 2009).

As an attempt to validate ocean models, a wide range of model-measurements comparisons (Oey et al., 1992; Hackett et al., 1995; Davies and Hall, 2002) and also hydrostatic model-model comparisons have been performed (Hackett et al., 1995; Røed et al., 1995; Avlesen et al., 2001) and also a non-hydrostatic comparison by Berntsen et al. (2006).

Through the Metocean Modeling Project, Røed et al. (1995) and Hackett et al. (1995) tried to choose the best ocean model out of six models. The evaluation was based on test cases suggested by Haidvogel and Beckmann (1998) and Smith et al. (1996). The simulations were done with a resolution ranging from 20 to 2500 meters, and quite large differences between the models were found. These differences were primarily considered generated by inadequate parametrization of subgrid processes, not sufficient horizontal resolution, and not well-defined boundary and initial conditions (Hackett et al., 1995).

In the hydrostatic study by Avlesen et al. (2001) a density driven plume affected by rotation was studied using the Princeton Ocean Model (POM) and Bergen Ocean Model (BOM). Convergence was achieved as the horizontal grid sizes were refined from 20 km to 2.5 km. Both POM and BOM use terrain-following coordinates, and the study was done using very high viscosities, hence interesting dynamics may have been filtered out. Additionally the study was performed with a flat bottom. Though the converging results are reassuring, more benchmarks also with lower viscosities are needed in order to sufficiently validate the quality of the two ocean models.

Berntsen et al. (2006) did non-hydrostatic numerical experiments on laboratory scales using the z-coordinate model the Massachusetts Institute of Technology general circulation model (MITgcm) and the σ-coordinate model Bergen Ocean Model (BOM) where they simulated two different test cases, tank experiments on lock-release flow and solitary waves propagating over a flat bottom approaching an incline. These simulations were high resolution experiments with horizontal resolutions ranging from 4 to $0.5{\cdot}10^{-4}$ m, using molecular viscosities, and they found good correlation between the two concerned ocean models. Still, in order to reduce the noise generated from the staircase topography, Berntsen et al. (2006) used the Shapiro filter at the end of each time step on the temperature and the velocity fields in the study of a solitary wave approaching an incline with the MITgcm.

In this paper flow over a backward-facing step is studied using the 2DV versions of the MITgcm and BOM. The sharp backward-facing step is the simplest reattaching flow (Simpson, 1996), and a known testcase for numerical models. It is often studied due to its simplicity combined with a separating boundary layer, bifurcation of the reattachment point, reattachment of the flow, and recovery of the boundary layer (Hanjalić and Jakirlić, 1998). Large eddies with at least the length scale of the step occur in the recirculating region (Eaton and Johnston, 1981). A wide range of studies of the reattachment length have been performed, and Armaly et al. (1983) gives a nice summary.

Laboratory experiments have been carried out and give us valuable data for numerical tests (Kim et al., 1985; Lee and Mateescu, 1998; Fessler and Eaton, 1999; Beaudoin et al., 2004; Nie and Armaly, 2004; Song and Eaton, 2004). Model experiments have also been done on flow over a backward-facing step, both through Direct Numerical Simulations (Le et al., 1997), Large Eddy Simulations (Akselvoll and Moin, 1996), and Reynolds Averaged Navier Stokes models (Lee et al., 2009).

As for the case of the rounded step, the separation occurs slightly downstream of the beginning of the topographic change (Wasistho and Squires, 2005) and is determined by the adverse pressure gradient generated by the increasing depth. The rounded step has been studied, both through experiments (Bravo and Zheng, 2000; Song et al., 2000; Bao and Dallmann, 2004; Hoefener and Nitsche, 2008) and numerical simulations (Bravo and Zheng, 2000; Neumann and Wengle, 2003, 2004; Wasistho and Squires, 2005; Chen et al., 2006).

There exists a much broader literature on flow over a sharp step compared to flow over a rounded step. Though the backward-facing step has been studied extensively, understanding and modeling separation and reattachment within the turbulent regime are still a problem (Song and Eaton, 2004).

This paper can be considered as an extension of the comparison by Berntsen et al. (2006) to larger scales using constant eddy viscosities but with the aim to resolve physical boundary layer processes. The main focus is on the separation point, the reattachment length, and the mean velocity at the bottom behind the step. The paper presents both instantaneous states and averaged states of the flow.

The grid sizes in this study are in the range between laboratory scales often simulated using Direct Numerical Simulations resolving the Kolmogorov scales, and ranges traditionally studied using Reynolds Averaged Navier-Stokes models with grid sizes of kilometers. The length scales in this paper are chosen in order to explore whether the models are able to represent complex flow also at this range.

2 Models and setup

The simulations of flow over a backward-facing step are done using two different general circulation models, the z-coordinate model, the Massachusetts Institute of Technology general circulation model, MITgcm (Adcroft et al., 2008), and the σ-coordinate model Bergen Ocean Model, BOM (Berntsen, 2004).

2.1 Governing equations

The basic equations are the Reynolds averaged momentum equations averaged both in time and space. Additionally the Boussinesq approximation is used leading to an inclusion of the density changes only in the gravity term. Rotation has been neglected, giving the following momentum equations,

$$\frac{\partial U}{\partial t} + \frac{\partial U^2}{\partial x} + \frac{\partial UW}{\partial z} = -\frac{1}{\rho_0}\frac{\partial P}{\partial x} + \frac{\partial}{\partial x}(A_M \frac{\partial U}{\partial x}) + \frac{\partial}{\partial z}(K_M \frac{\partial U}{\partial z}) \,, \tag{1}$$

$$\frac{\partial W}{\partial t} + \frac{\partial UW}{\partial x} + \frac{\partial W^2}{\partial z} = -\frac{1}{\rho_0}\frac{\partial P}{\partial z} - \frac{\rho g}{\rho_0} + \frac{\partial}{\partial x}(A_M \frac{\partial W}{\partial x}) + \frac{\partial}{\partial z}(K_M \frac{\partial W}{\partial z}) \,. \tag{2}$$

Incompressibility is assumed, and the equation of continuity can hence be written on the form,

$$\frac{\partial U}{\partial x} + \frac{\partial W}{\partial z} = 0 \,. \tag{3}$$

In Equation (1)-(3), $U(x, z, t)$ represents the horizontal velocity, $W(x, z, t)$ the vertical velocity, $P(x, z, t)$ the pressure, ρ the density, and ρ_0 a reference density. The flow is homogeneous with a density of 1028 kg m^{-3}. The constant

of gravity is represented by g, A_M is the horizontal eddy viscosity, and K_M the vertical eddy viscosity.

For the scalar properties, as the density, a conservation equation is used,

$$\frac{\partial \rho}{\partial t} + \frac{\partial U\rho}{\partial x} + \frac{\partial W\rho}{\partial z} = \frac{\partial}{\partial x}(A_H \frac{\partial \rho}{\partial x}) + \frac{\partial}{\partial z}(K_H \frac{\partial \rho}{\partial z}) \ , \tag{4}$$

where A_H represents the horizontal eddy diffusivity, and K_H the vertical eddy diffusivity.

The pressure at the depth z is expressed by,

$$P(x,z,t) = g\rho_0\eta(x,t) + g\int_z^0 \rho dz' + P_{NH}(x,z,t) \ , \tag{5}$$

where the first term represents pressure due to the surface elevation, the second term the internal pressure, and the last term is a non-hydrostatic correction term due to internal movements in the fluid. The non-hydrostatic pressure is found through an elliptic equation, and in BOM the elliptic equation for the non-hydrostatic pressure is solved using a successive over-relaxation (SOR) method. The iterations continue until the relative error measured in the 2-norm for the vector is less than 10^{-4} (Berntsen et al., 2006), or the number of iterations have reached 50. The MITgcm uses a preconditioned conjugated method, and this method is in general faster than the SOR-method used in BOM (Berntsen et al., 2006). Solving the elliptic equation for the non-hydrostatic pressure leads to approximately 4 times higher computational costs per time step compared to a hydrostatic simulation using BOM, when the relative error should be less than 10^{-4}. This computational cost is in correspondence with other methods as Fringer et al. (2006).

At the bottom a quadratic drag is used, specified by (Berntsen, 2004; Adcroft et al., 2008),

$$\boldsymbol{\tau}_x = \rho_0 C_D |U_b| U_b \ , \tag{6}$$

where U_b represents the velocity in the lowest grid cell above the bottom, and the drag coefficient, C_D, is set to $5.2{\cdot}10^{-3}$ in all simulations.

2.2 Closing the system

In order to close the system, values for the eddy viscosities and diffusivities must be chosen. On small scale, turbulence is isotropic, but on larger scale the turbulence is influenced by the turbulence macroscale (Kantha and Clayson, 2000). Berntsen et al. (2006) assumed isotropy, but in their study the coarsest simulations were done using a resolution of millimeters compared to meters in this paper.

In the DNS simulations by Le et al. (1997) and the LES simulations by Neumann and Wengle (2004) the Kolmogorov scales are resolved and isotropic turbulence is assumed, while in the RANS-study by Lee et al. (2009) the $k-\epsilon$ model is used to determine the eddy viscosities and diffusivities.

In the experiments with BOM, the horizontal eddy diffusivity is set to 0 in order to avoid unphysical mixing near the slopes (Mellor and Blumberg, 1985). In the simulations with the MITgcm the horizontal eddy viscosities and diffusivities are set to the constant value of 10^{-2} m^2 s^{-1}. Though it would have been desired to have an even lower value for the horizontal eddy viscosity and diffusivity, this is the lowest value that ensures numerical stability for both models.

In the vertical, fixed values for the eddy viscosity and diffusivity ranging from 10^{-2} m^2 s^{-1} to 10^{-6} m^2 s^{-1} are used. Though the horizontal eddy diffusivities and viscosities are higher than the vertical values, the closure is in correspondence with values set by (Xing and Davies, 2006; Berntsen et al., 2009) for corresponding resolutions.

2.3 Topographic setup

2DV simulations of flow over a backward-facing step are presented, where all variables are normalized based on the step height, h, and the free-stream velocity, U_∞. A sketch of the setup for flow over a backward-facing step can be found in Figure 1. The total length of the domain is 900 meters, and the domain is discretized into an equidistant horizontal grid with resolutions from 6 to 1.5 meters. The vertical grid is also equidistant, with a resolution ranging from 1 meter to 0.25 meter before the step. The rounded step starts at $x = 0$.

Haney (1991) discussed the internal pressure error related to σ-coordinates. The internal pressure error is caused by the x-component of the internal pressure written in σ-coordinates (Haney, 1991),

$$\frac{\partial p}{\partial x}\Big|_z = \frac{\partial p}{\partial x}\Big|_\sigma - \frac{\sigma}{D}\frac{\partial D}{\partial x}\frac{\partial p}{\partial \sigma}\,. \tag{7}$$

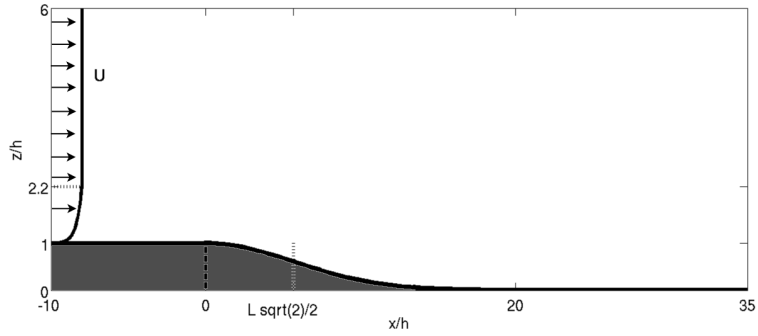

Fig. 1 The setup of the backward-facing step. At the left boundary the velocity profile is prescribed with a free stream velocity of $U_\infty = 0.1\text{m}^2\text{s}^{-1}$ above a logarithmic layer of $\delta = 1.2h$. The height of the step is given by $h = 20$ m. The vertical height of the domain is set to $6h$, and the horizontal extent to $45h$. The distance from the left boundary to the step is set to $10h$, and the turning point of the slope is located in $L\frac{\sqrt{2}}{2}$.

Here p represents the pressure, D the total depth of the domain including the surface elevation, and $\sigma \equiv \frac{z}{D}$. When the σ-coordinates are discretized on steep topography the two terms on the right hand side may be large, of the same magnitude, and of opposite signs. This can cause large errors in the internal pressure estimate (Berntsen, 2002).

The topography of the rounded step is described by,

$$H(x) = \begin{cases} -100\ , & x < 0\ , \\ -120 + h \cdot \exp^{-\frac{x^2}{(Lh)^2}}\ , & x \geq 0\ , \end{cases} \tag{8}$$

where the left boundary is located at $x = -10h$. Two different slopes have been studied, defined by setting $L = 3$ or $L = 8$. The step height, h, is set to 20 m. The ratio of the depth, length and step height is chosen based on corresponding simulations by Neumann and Wengle (2004).

In this paper the results are presented by the Reynolds number, calculated according to,

$$Re = \frac{U_\infty h}{\nu}\ , \tag{9}$$

where U_∞ represents the free stream velocity set to 0.1 m s^{-1}, h the height of the step, and ν the viscosity. Since the horizontal eddy viscosity is set to 10^{-2} m^2 s^{-1} for all simulations and filters out the numerical noise, the vertical eddy viscosity is used for calculating the Reynolds number. The Reynolds number then varies between $2{\cdot}10^2$ and $2{\cdot}10^6$ based on these assumptions. The Reynolds number estimated from the horizontal viscosity is $2{\cdot}10^2$ in all simulations.

Simulations of the MITgcm and flow over a sharp step compared to published literature are presented in Appendix A.

2.4 Initial and boundary conditions

Initially the velocity profile is defined by a depth integrated velocity leading to a horizontal flux of 10 m^2 s^{-1}. This flux gives an average free-stream velocity of U_∞=0.1 m s^{-1} for the shallowest area before the step.

At the inflow, the velocities are prescribed by a logarithmic layer in the boundary layer. The velocities within the boundary layer are described by the equation,

$$U_{bl}(z') = \frac{u_*}{k}\ln z' + C\ , \tag{10}$$

where z' is the distance from the bottom, the friction velocity u_* is approximated as $u_* = U_\infty/30$, and C is a constant chosen to satisfy $U_{bl}(\delta) = U_\infty$. The thickness of the boundary layer is set to $\delta = 1.2h$, in correspondence with the experiments by Jovic and Driver (1995), Akselvoll and Moin (1996), and Le et al. (1997).

For the MITgcm the prescribed value option is used in order to describe the inflow velocities. The open boundaries in Bergen Ocean Model are set using

the Flow Relaxation Scheme (FRS) described by Martinsen and Engedahl (1987). The FRS-zone consists of the 7 horizontal cells at the boundary. At the outflow boundary, the velocity and the density are set to the mean values of the seven cells inside the FRS-zone from the same layer. In the MITgcm the passive Orlanski radiation condition (Adcroft et al., 2008) has been used at the outflow boundary.

There is not done any Shapiro filtering related to the staircase topography in the MITgcm. This option is chosen to better compare the results generated by the core of the two models, and to not suppress any non-hydrostatic behavior due to filtering.

3 Results and discussions

The bottom boundary layer is affected by, among other factors, the pressure gradient and the wall curvature. As the depth increases an adverse pressure gradient is generated due to the Bernoulli dynamics. If the adverse pressure gradient is large enough his can lead to negative velocities within the boundary layer and hence separation of the flow. Results using two different slopes of the rounded step, $L = 3$ and $L = 8$ (Equation (8)) are presented.

3.1 Separation and reattachment

To make sure that the bottom boundary layer is fully resolved and developed in all simulations, the thickness of the δ_{90} layer have been calculated. The δ_{90} layer represent the distance from the bottom to the vertical position where the horizontal velocity equals $0.9U_\infty$ (Kundu and Cohen, 2004), and is found to vary by only plus minus one grid cell as the backward-facing step is approached.

For a rounded step, the separation point is determined by the adverse pressure gradient, the viscous forces, and the velocity profile. For high Reynolds numbers the flow is characterized by instability (Bao and Dallmann, 2004; Wasistho and Squires, 2005). The characteristics of the flow can therefore not be studied using instantaneous properties. The mean reattachment point and separation point are hence defined as the point where the average horizontal velocity between 12 and 24 hours is zero, and is found by searching for a shift in sign in the average bottom velocities in the defined period. This is a definition in correspondence with Kasagi and Matsunaga (1995), and assumes that long-time averaged values can be compared, also an assumption made by Hanjalić and Jakirlić (1998).

Table 1 and 2 show the mean separation point and the mean reattachment point for the two different steepnesses of the slopes. For Reynolds number of $\mathrm{Re}=2{\cdot}10^2$ the viscous forces are larger than the adverse pressure gradient for both slopes, and the pressure gradient generated by the change in topography is not large enough to cause separation of the flow.

Table 1 The average reattachment point and separation point using a slope of L=3. The second column gives the number of grid cells used in the simulations, where the first number represents the horizontal number of grid cells, and the last number the vertical number of grid cells. The third column gives the numerical model and column four to seven give the average separation point or reattachment length.

Re			$2{\cdot}10^3$	$2 \cdot 10^4$	$2 \cdot 10^5$	$2 \cdot 10^6$
Separation	150x100	BOM	-	2.6	1.7	1.7
	300x200	BOM	-	1.7	-0.70	-1.2
	600x400	BOM	-	1.8	-0.44	-2.2
	150x100	MITgcm	2.9	1.7	1.4	1.1[a]
	300x200	MITgcm	2.5	1.4	1.4	1.4[b]
	600x400	MITgcm	2.3	1.3	1.1	1.2
Reattachment length	150x100	BOM	-	18.5	14.9	14.3
	300x200	BOM	-	12.1	7.6	7.1
	600x400	BOM	-	12.3	4.8	5.5
	150x100	MITgcm	10.4	13.1	9.2	10.7
	300x200	MITgcm	14.5	10.3	10.6	10.4
	600x400	MITgcm	15.4	10.0	10.0	9.5

[a] Negative values occur at $x = -6.7$.
[b] Negative values occur at $x = -7.0$.

For Reynolds number of Re=$2{\cdot}10^3$, separation occur for the steepest slope, $L = 3$ using the z-coordinate model, MITgcm. This separation vortex is stationary and in correspondence with the stationary separation bubble found by Bao and Dallmann (2004) for Reynolds numbers of 2700. Using BOM there is no separation of the flow. One explanation for this deviation might be higher numerical damping in BOM compared to the MITgcm, caused by for instance

Table 2 The average reattachment length and separation point for a slope of L=8. The second column gives the number of grid cells used in the simulations, where the first number represents the horizontal number of grid cells, and the last number the vertical number of grid cells. The third column gives the numerical model and column four to seven give the average separation point or reattachment length.

Re			$2{\cdot}10^3$	$2 \cdot 10^4$	$2 \cdot 10^5$	$2 \cdot 10^6$.
Separation	150x100	BOM	-	5.9	4.1	3.8
	300x200	BOM	-	5.3	1.4	0.80
	600x400	BOM	-	5.8	2.1	2.6
	150x100	MITgcm	-	6.2	6.2[a]	6.8
	300x200	MITgcm	-	5.2	3.9	3.5[b]
	600x400	MITgcm	-	5.5	4.6	3.4
Reattachment length	150x100	BOM	-	21.2	17.6	17.0
	300x200	BOM	-	15.4	8.15	13.0
	600x400	BOM	-	10.5/18.0[b]	11.0	11.6
	150x100	MITgcm	-	16.1	16.7	17.3
	300x200	MITgcm	-	16.4	14.3	13.7
	600x400	MITgcm	-	16.5	13.3	12.2

[a] Negative velocities are observed at $x = -7.0$.
[b] Two eddies occur on the slope.

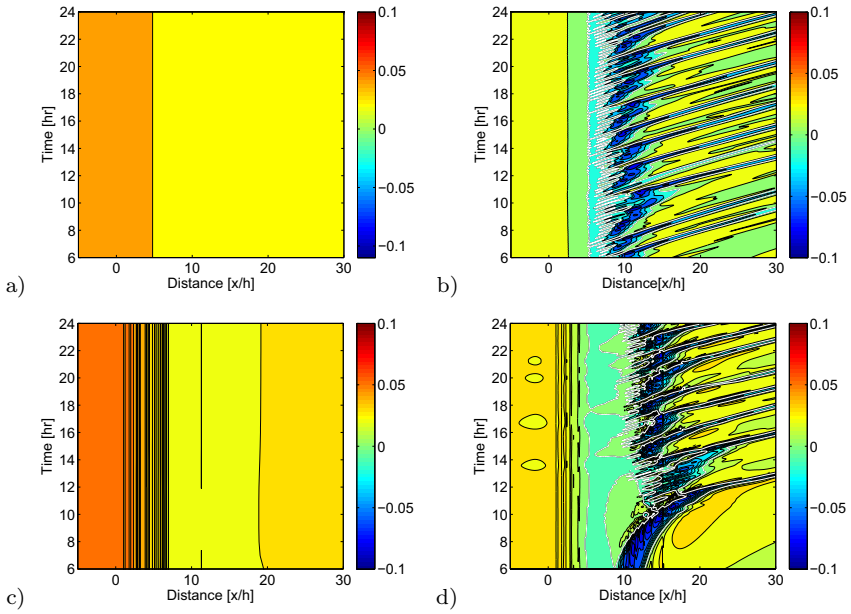

Fig. 2 The horizontal bottom velocities for a slope of L =8 and 300x200 grid cells using: a) BOM, Re=$2{\cdot}10^3$ b) BOM Re=$2{\cdot}10^4$, c) MITgcm Re=$2{\cdot}10^3$, and d) MITgcm Re=$2{\cdot}10^4$. The white line represents the locations where the horizontal velocity equals 0.

the implicit method used as a corrector in the time stepping in BOM (Berntsen et al., 2006).

Separation occurs in all simulations for Reynolds numbers higher than or equal to Re=$2{\cdot}10^4$. Using the z-coordinate model, and a slope of $L = 3$, the reattachment point varies between $x/H \in [9.6, 10.5]$, however using the σ-coordinate model and Re$\geq 2 \cdot 10^5$ the separation point and the reattachment zone is shifted upstream with increasing resolution and does not converge. For these Reynolds numbers the separation occurs before the step with BOM. For the less steep case (L=8) the MITgcm estimates a mean reattachment length of approximately 16.5 for Reynolds numbers of Re= $2{\cdot}10^4$, but also the MITgcm model encounters convergence problems for Reynolds numbers higher than $2 \cdot 10^5$.

3.2 Time dependency

Figure 2 shows the horizontal bottom velocities from 6 to 24 hours for Re=$2{\cdot}10^3$ and Re=$2{\cdot}10^4$ using $L = 8$ and 300x200 grid cells. For the lowest Reynolds number the flow is stationary both for the MITgcm and BOM (Figure 2 a) and c)), and there is no separation of the flow (in correspondence with Bao and Dallmann (2004)'s results). The staircase topography from the z-coordinate model causes noise. This can be observed in Figure 2 c) as the variation in the horizontal velocity between x/h=2 and x/h=7.

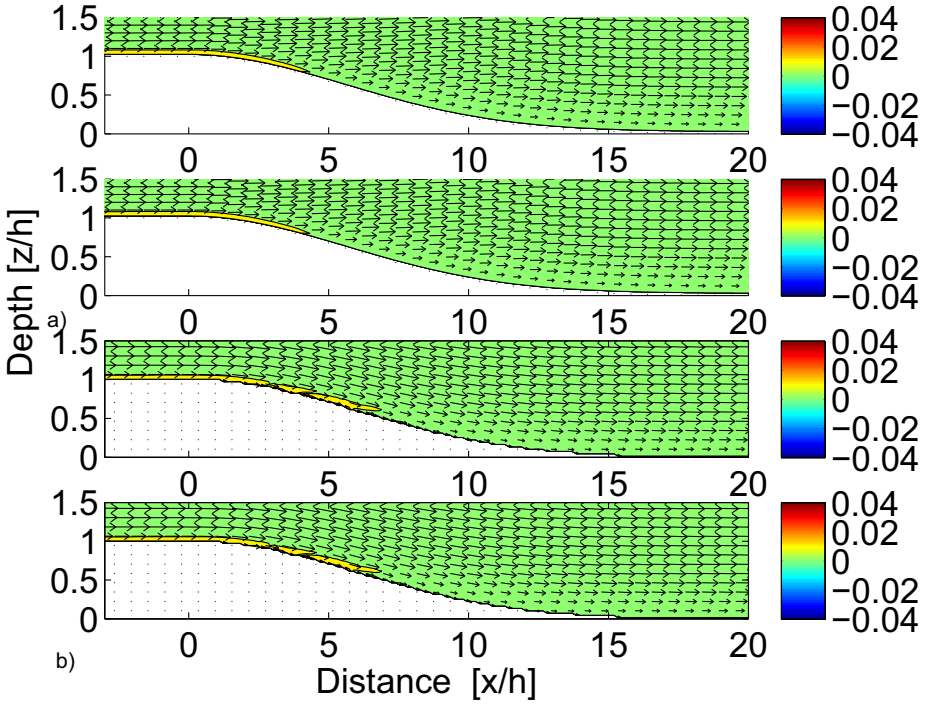

Fig. 3 The mean vorticity and the mean velocity arrows from 12 to 24 hours and a snapshot of the vorticity and the velocity arrows at 24 hours for Re=$2{\cdot}10^3$ using a) BOM and b) MITgcm.

For Re=$2{\cdot}10^4$, eddies are generated on the slope due to the adverse pressure gradient for both models. The separation point is located between x/h=5.2-5.3 (Figure 2 b) and d)) and is quite constant in time. Downstream the separation point there is a region with very low velocities, before a region with high negative velocities can be observed. The high negative velocities are related to clockwise eddies. These eddies are generated directly downstream the separation region and are eventually released from the recirculation zone. As one vortex is moved downstream new vortex structures are generated just downstream from the separation line. This phenomenon is also observed in Bao and Dallmann (2004)'s studies. Due to the vortex shedding, the reattachment point fluctuates in time (Eaton and Johnston, 1981). The vortex shedding can give an instantaneous change in reattachment point of several step heights (Simpson, 1996). The fluctuating reattachment point can be seen by the saw-tooth pattern in Figure 2 b) and d).

The region just downstream of the separation point with very low velocities (Figure 2 b) and d)) is often referred to as "the dead-water region" (Bao and Dallmann, 2004). This region is larger using the MITgcm compared to BOM.

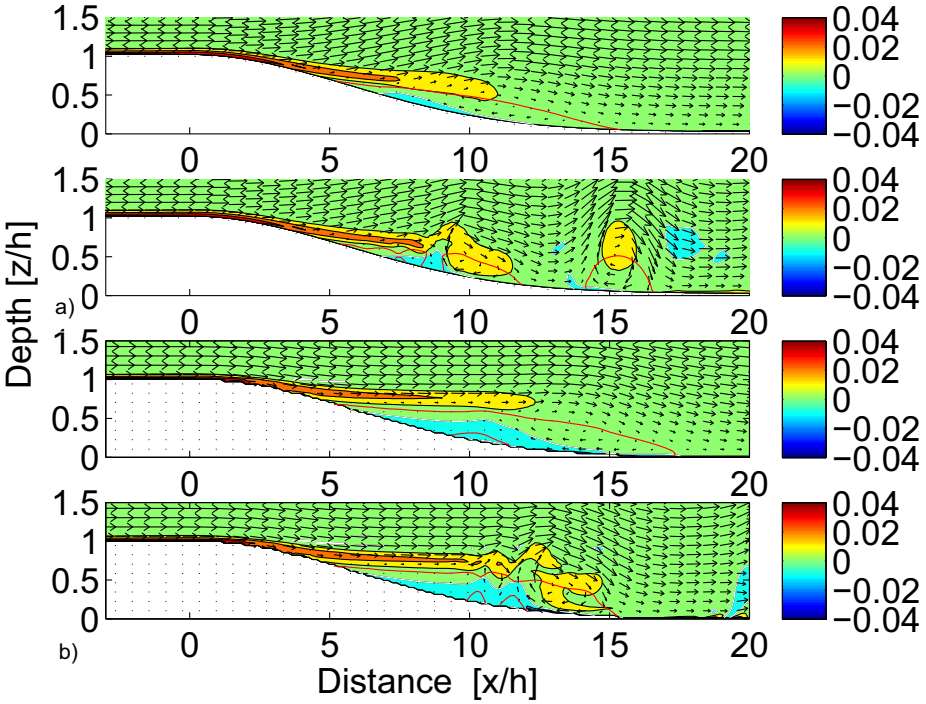

Fig. 4 The mean vorticity and the mean velocity arrows from 12 to 24 hours and a snapshot of the vorticity and the velocity arrows at 24 hours for Re=$2{\cdot}10^4$ using a) BOM and b) MITgcm. The red line represents where the horizontal velocity equals 0.

3.3 Effects of the vertical discretization methods, resolution and Reynolds numbers

Figure 3-5 show the mean vorticity between 12 and 24 hours using Re=$2{\cdot}10^3$, $2{\cdot}10^4$, and $2{\cdot}10^6$ for both ocean models and a slope of $L = 8$. The top figure shows the mean vorticity and the lower figure a snapshot of the vorticity after 24 hours of simulation.

The stationarity of the flow within the laminar regime, Re=$2{\cdot}10^3$, is illustrated in Figure 3. For the simulations with Re=$2{\cdot}10^4$ both MITgcm and BOM give a clockwise eddy behind the separation point when the mean vorticity is calculated from the average velocity field in the last 12 hours of the simulation (Figure 4). However the height of the eddy is smaller using BOM compared to the MITgcm. Looking at the snapshot of the vorticity, one can observe that the eddies are generated further upstream in the terrain-following model compared to in the z-coordinate model. The reduction of the height of the separation bubble and also the shift upstream in separation point are especially prominent as the vertical eddy viscosities are reduced to 10^{-6} m^{2}s^{-1} (Figure 5). In the latter case the stagnant eddy is now replaced by a number of

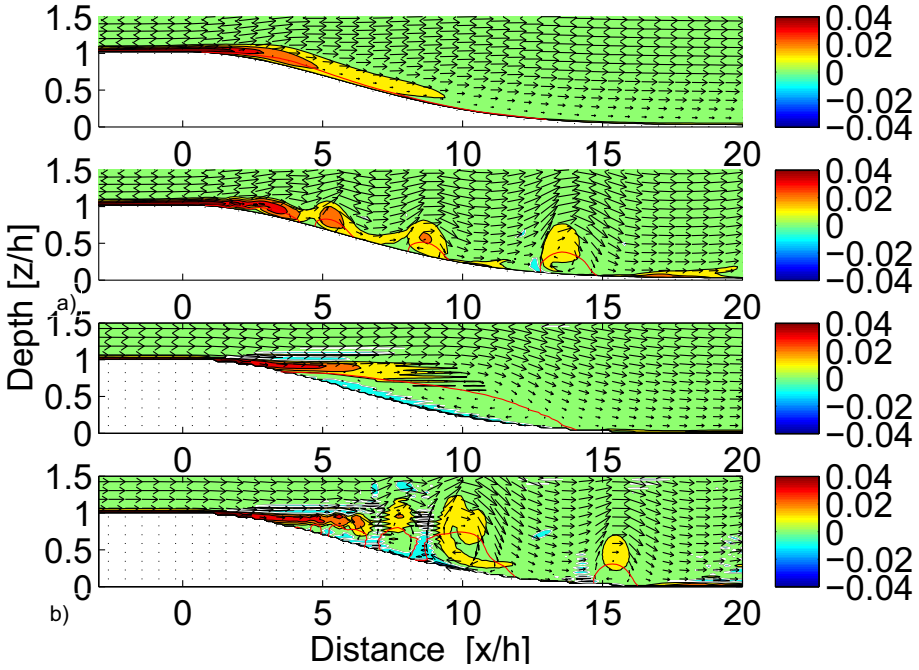

Fig. 5 The mean vorticity and the mean velocity arrows from 12 to 24 hours and a snapshot of the vorticity and the velocity arrows at 24 hours for Re=$2{\cdot}10^6$ using a) BOM and b) MITgcm. The red line represents where the horizontal velocity equals 0.

smaller eddies on the slope. Bao and Dallmann (2004) observed a reduction in the spatial size of the vortexes for increasing Reynolds numbers. However the separation line in the experiments by Bao and Dallmann (2004)'s experiments is more horizontal than what is found in the simulations with vertical eddy viscosities of 10^{-6} $\mathrm{m^2 s^{-1}}$ using BOM.

The normalized wall skin friction coefficient is defined as,

$$C_f = \frac{\tau_w}{\frac{1}{2}\rho U_\infty^2} \,, \tag{11}$$

where τ_w represents the wall shear stress (Le et al., 1997). The skin friction coefficient in the simulations with $L = 8$ and a Reynolds number $2{\cdot}10^4$, and $2{\cdot}10^6$ with a resolution of 300x200 grid cells is presented in Figure 6. Negative peaks in the skin friction coefficient is observed within the recirculating region. The magnitude of the negative peak skin friction coefficient within the recirculating region is approximately the same using BOM compared to the MITgcm. The low skin friction just downstream the separation point, correspond to the low velocity region or "dead-water region". However the magnitude of the skin friction coefficient is lower than in the studies by Le et al. (1997) and Chen et al. (2006). This can be explained by the much larger scales in this setup, with a height of the step of meters compared to cm, leading to a less resolved

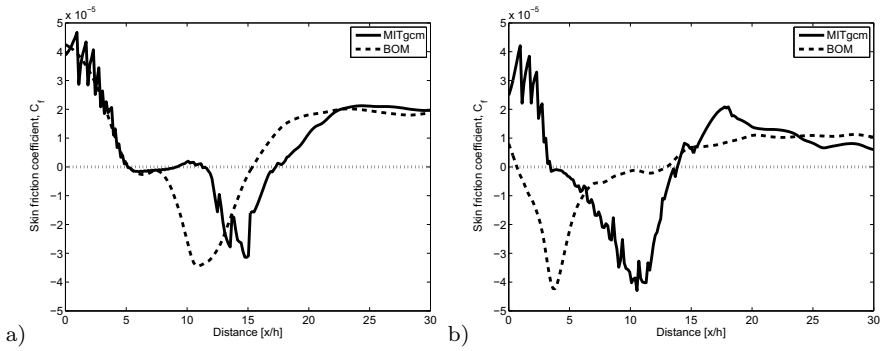

Fig. 6 The skin friction for the simulations with L=8 for a resolution of 300x200 grid cells a) Re=$2{\cdot}10^4$ and b) Re=$2{\cdot}10^6$.

sharp velocity gradient near the bottom. In addition Bravo and Zheng (2000) reported a reduction in the magnitude of the skin friction coefficient for flow over a rounded step compared to a sharp step. As in Le et al. (1997) the skin friction coefficient increases with decreasing Reynolds number in the recovery region (Figure 6).

The Strouhal number, $St = \frac{fh}{U_\infty}$, is approximately 0.03 for the simulations with vertical eddy viscosities of $10^{-4}\mathrm{m}^2\mathrm{s}^{-1}$, when f is the average frequency of vortex shedding and h the height of the slope. As the vertical eddy viscosity is reduced to $10^{-6}\mathrm{m}^2\mathrm{s}^{-1}$ the Strouhal number increases to 0.06 for the simulations with BOM, but is still approximately 0.03 in the simulations using the MITgcm. For the direct numerical simulations of a sharp backward-facing step Le et al. (1997) reports a Strouhal number of 0.06.. The increase in Strouhal number with increasing Reynolds number (observed in BOM) is previously reported by Bao and Dallmann (2004).

In BOM there has been used values of the horizontal diffusivity of 0 compared to 0.02 $\mathrm{m}^2\mathrm{s}^{-1}$ in the MITgcm. Setting the horizontal eddy diffusivity to 0.02 $\mathrm{m}^2\mathrm{s}^{-1}$ also in BOM, only gives a minor shift in the position of the reattachment point. The important parameters in this setup are the vertical coordinate, the grid size and the vertical eddy viscosity. As Δx is less or equal to 3 m the length of the reattaching region is reduced for high Reynolds numbers ($\geq 2 \cdot 10^5$). This reduction in reattachment length for higher Reynolds numbers is also observed by Song and Eaton (2004). The length of the reattachment zone is also reduced as the vertical viscosity is reduced from $10^{-4}\mathrm{m}^2\mathrm{s}^{-1}$ to $10^{-5}\mathrm{m}^2\mathrm{s}^{-1}$.

Using a horizontal resolution of 6 m (150x100 grid cells), the separation point and reattachment point is less dependent on the viscosity for both models. At this resolution the numerical viscosity influences the solution. The staircase topography in the MITgcm forces the reverse flow to propagate in the vertical direction as the rear current faces a vertical wall. Hence noise occurs, leading to enhanced bottom mixing. In BOM the topography is smooth, and the velocity is less influenced by bottom noise. As the horizontal reso-

lution is reduced to 3 meters or less, the recirculating bubble is shifted upstream in BOM due to reduced numerical viscosity, and also lower frictional effects compared to the MITgcm. Using the MITgcm the size of the eddies are less influenced by the Reynolds number and the resolution due to the increased mixing caused by the the staircase topography. The mixing related to the steps is independent of the background viscosity, making the bottom flow in the MITgcm less dependent on the Reynolds number than in BOM. Also Wasistho and Squires (2005) reports variations in the estimates of the reattachment length when different RANS models are used, illustrating the complexity of modeling separating flow.

In order to improve the correlations between the flow fields in BOM and MITgcm one must either use a much higher resolution to directly resolve all the structures on the slope or a parametrization of the sub-grid processes. However the latter is outside the scope of this work since it will not compare the core of the two models.

3.4 Round step versus sharp step

There exists a much wider literature of flow over a sharp step compared to a rounded step. Simulations of flow over a sharp step using the MITgcm have hence been performed in order to compare the results to published literature. The results can be found in appendix A. For flow over a sharp step, the separation point is located at the edge of the step. Downstream the separation point there are many similarities between flow over a rounded step and over a sharp step. The MITgcm is able to represent flow patterns over a sharp step both within the laminar, the transition and the turbulent regime. A horizontal resolution of $\Delta x = 3$ m gives the best results compared to literature, and a resolution of $\Delta x \leq 6$ m is needed in order to achieve robust results. As for the rounded step increasing resolution and Reynolds number lead to more and more eddies generated downstream the step. In addition the release time for the eddies are also reduced as the resolution and Reynolds number are increased.

3.5 3-dimensionality

Flow over a backward-facing step has three-dimensional properties. Still in order to achieve high resolution, the study is done in two dimensions. There exists a wide range of 2DV studies, especially for flow over a sharp step. For the sharp backward-facing step, three dimensional effects are observed for Reynolds number greater than 400 (Williams and Baker, 1997). It has been found an underestimation of the reattachment length for two-dimensional studies for Reynolds numbers larger than 400 m for the sharp step (Williams and Baker, 1997).

According to Bao and Dallmann (2004) the eddies keep their two-dimensional features only for a short distance downstream the separation point. A short

distance after the separation point the eddies start to twist and stretch (Bao and Dallmann, 2004). 2DV simulations hence give more robust results of the separation point than the reattachment point. In this study the flow is modeled using 2DV versions of the respective models in order to ensure high resolution. In the future, the study should be extended in the y-direction in order to include how three-dimensional phenomena will affect the separation point and the reattachment point. Deviations from the published results might be due to the fact that in 2DV simulations the vortex stretching mechanism in the y-direction is lost (Ting et al., 2006). This will influence both the velocity and the energy fields, and energies can hence be accumulated at the wrong scales (Ting et al., 2006).

4 Summary

In order to understand the separating flow over a rounded step it is important to resolve the vortexes downstream of the separation point properly. Bao and Dallmann (2004) observed a steady separation point, and a steady angle between the separation line and the wall. Downstream the separation point the flow pattern is complex for Re$>$ 2700 with many downstream moving vortexes in the separated flow region (Bao and Dallmann, 2004). This phenomenon is also observed through this study with a stationary flow without separation for low Reynolds number, a stationary separation bubble using the MITgcm for Re$=2 \cdot 10^3$ and $L = 3$, and time-dependent flow with separation for Reynolds number higher than or equal to Re$=2 \cdot 10^4$ for both slopes.

The vertical discretization in the models influences the results. The staircase topography in the MITgcm enhances the mixing and leads to an increased height of the reattachment zone compared to the terrain-following model. The flow simulated with the MITgcm is more affected by noise from the topography than the flow in BOM, leading to smoother eddies on the slope when flow over a backward-facing step is modeled by BOM for high Reynolds numbers. The rear flow in the z-coordinate mode is affected by the staircase topography, leading to a more stagnant separation point and reattachment point than in the σ-coordinate model. In BOM the separation point occurs before the onset of step for the case of the steepest slope L=3. If increased values of the eddy viscosity and diffusivity is included in the lowest layer at the slope in BOM, the separation point is shifted downstream.

As Bao and Dallmann (2004), an increase in the frequency of vortex shedding for enhanced Reynolds number is found. Using BOM also the sizes of the vortexes are reduces spatially as the Reynolds number increases in correspondence with Bao and Dallmann (2004). However the separation line is more horizontal in Bao and Dallmann (2004)'s experiments than in the simulations using BOM for high Reynolds numbers. The vortex shedding frequency is of the same size as in Le et al. (1997)'s direct numerical simulation of flow over a sharp step using vertical eddy viscosities of 10^{-6} m^{2}s^{-1} and BOM. For lower Reynolds numbers and in the simulations with the MITgcm the vor-

tex frequency is up to 50% lower than in Le et al. (1997)'s Direct Numerical Simulations.

BOM gives the benefit of smoother eddies less influenced by noise caused by the topography, while the MITgcm gives a more robust average separation point and reattachment length without the use of complex turbulence schemes, and also a more horizontal separation line. However in the presence of a proper turbulence scheme BOM will probably be better suited than the MITgcm to simulate the flow on the step without the interaction of noise from the topography.

5 Acknowledgment

The work is supported by the European Project EU IP CarboOcean (511176-2) and The Research Council of Norway through NFR 146526/420: Cordino.

A Sharp step

The backward-facing sharp step is a well-known testcase for numerical models. Many laboratory experiments and numerical simulations have been performed and published and can be used for validation of numerical models. In this appendix results of simulations of flow over a sharp step using the MITgcm are presented. The results from these simulations are then compared to published literature.

A.1 Setup

The topography $H(x)$ is described by,

$$H(x) = \begin{cases} -100\,, & x < 0\,, \\ -120\,, & x \geq 0\,, \end{cases}$$

and the left boundary is located at $x = -18h$. The velocity profile is defined by a depth integrated velocity of 10 $m^2\ s^{-1}$, leading to an average free-stream velocity of U_∞=0.1 m s^{-1} for the shallowest area. The step height, h, is set to 20 m, as for the rounded step. In correspondence with the simulations of the rounded step the horizontal eddy viscosity and diffusivity is set to 10^{-2} $m^2\ s^{-1}$ in all simulations, and the vertical eddy viscosities and diffusivities are ranging from 10^{-2} $m^2\ s^{-1}$ to 10^{-6} $m^2\ s^{-1}$. The horizontal resolution varies from to 12 m to 1.5 m, leading to a total number of runs of 20.

A.2 Results and discussion

Figure 7 shows the mean streamlines from 12-24 hours (upper figure) and a snapshot of the streamlines (lower figure) after 24 hours of simulation for five different viscosities and two different grid sizes. For the lowest viscosities and diffusivities (10^{-2} $m^2\ s^{-1}$) corresponding to a Reynolds number of $2{\cdot}10^2$, the flow is stationary. The stability of the flow can be seen by the similarity between the average flow field and the snapshot of the velocity profile after 24 hours in Figure 7 a) and b). For higher Reynolds number the flow is time dependent and clockwise eddies are released from the reattachment zone and propagates downstream. For Reynolds number of $2{\cdot}10^3$ the reattachment zone is larger than for Reynolds number larger

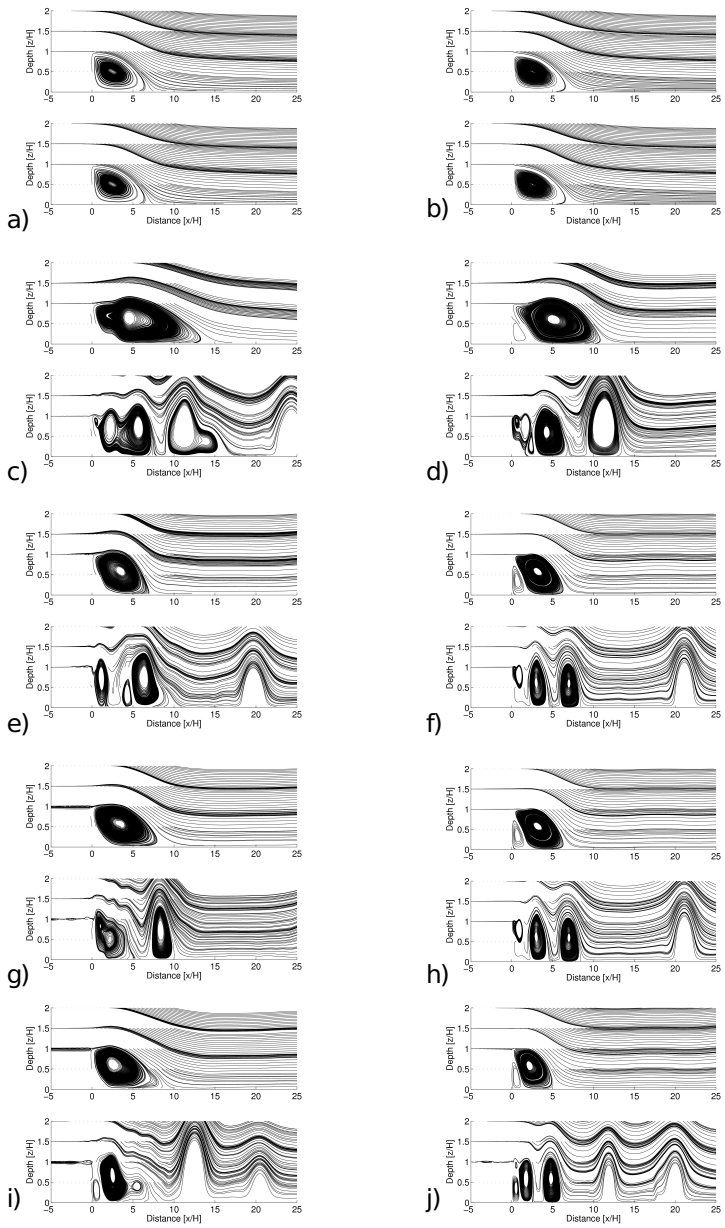

Fig. 7 Stream lines for the mean velocity field from 12-24 hours and a snapshot of the velocity field at 24 hours. The left column shows results using a resolution of 150x100 grid cells, and the right column results using a resolution of 300x200 grid cells, for a-b) $Re = 2{\cdot}10^2$, c-d) $Re = 2{\cdot}10^3$, e-f) $Re = 2{\cdot}10^4$, g-h) $Re = 2{\cdot}10^5$, and i-j) $Re = 2{\cdot}10^6$.

Table 3 The end of the first and the second eddies as a function of Reynolds number and numerical resolution. The second column gives the number of grid cells used in the simulations, where the first number represents the horizontal number of grid cells, and the last number the vertical number of grid cells. Column three to seven gives the length of the first and the second eddy in the recirculation region.

Re		$2 \cdot 10^2$	$2 \cdot 10^3$	$2 \cdot 10^4$	$2 \cdot 10^5$	$2 \cdot 10^6$
End 1st eddy	75x50	-	1.2	1.2	0.60	-
(Counter-clockwise)	150x100	-	0.90	1.5	1.8	1.5
	300x200	-	2.1	1.8	1.7	1.5
	600x400	-	3.8	1.6	1.2	1.3
End 2nd eddy	75x50	6.0	15.6	10.2	9.0	11.4
(Clockwise)	150x100	6.6	14.1	6.9	9.6	8.4
	300x200	6.8	11.1	6.6	6.6	5.3
	600x400	7.0	12.5	5.7	4.5	5.3

or equal to $2{\cdot}10^4$. According to Nie and Armaly (2004), flow over a backward facing step can be divided into three different regimes, laminar flow $Re < 400$, the transition flow regime $400 < Re < 3400$, and the fully turbulent flow regime $Re > 3400$. In the transition regime, Nie and Armaly (2004) observed a longer reattachment zone than in the fully turbulent regime, and in the turbulent regime the reattachment length was approximately constant (Nie and Armaly, 2004). As the grid sizes decrease (the right hand column in Figure 7) more eddies are resolved. Additionally the reattachment zone is elongated especially closer to the bottom boundary, where it tends to have a "tail" near the bottom for lower resolutions.

Table 4 Values of the reattachment length found in literature. Column 1 gives the reference, column 2 determines if it is a numerical simulation or a laboratory experiment, column 3 gives the Reynolds number, and the last column the reattachment length.

Reference	Calc/Exp	Re	Reattachment length
Gartling (1990)	Calc	600	12.2
Gartling (1990)	Calc	800	6.1
Akselvoll and Moin (1996)	Calc	38000	9.4
Kaiktsis et al. (2006)	Calc	2000	18.5
Le et al. (1997)	Calc	5100	6.28
Hanjalić and Jakirlić (1998)	Calc	5000	6.38
Chiang and Sheu (1999)	Calc	1000	12.75 [a]
Barkley et al. (2002)	Calc	600	11.41
Neumann and Wengle (2004)	Calc	3000	5.8
Beaudoin et al. (2004)	Calc	100	7
Rani et al. (2007)	Calc	1000-2000	10-13
ul Haque et al. (2007)	Calc	3615	6.42
Kim et al. (1985)	Exp	$3{\cdot}10^4$	7.0
Kim et al. (1985)	Exp	$4.5{\cdot}10^4$	7.0
Armaly et al. (1983)[b]	Exp	$70 < Re < 8000$	7.0
Armaly et al. (1983)	Exp	2000	13.5
Jovic and Driver (1994)	Exp	5100	6.0
Kasagi and Matsunaga (1995)	Exp	5540	6.51
Lee and Mateescu (1998)	Exp	≤ 3000	6.0
Fessler and Eaton (1999)	Exp	18400	7.4
Beaudoin et al. (2004)	Exp	100	4.5

[a] mean value from their simulations

[b] Results taken from Lee and Mateescu (1998)

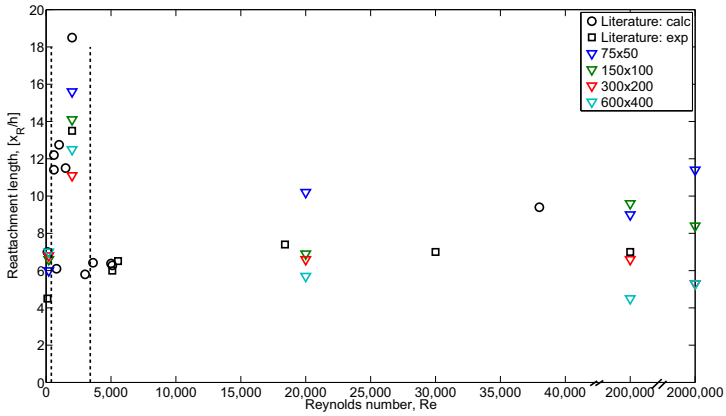

Fig. 8 Reattachment length versus Reynolds number. The black circles and squares represent values found from literature (Table 4). The triangles are modeled results presented in this paper (Table 3). The vertical dotted black lines divide the results into the laminar regime, the transition regime, and the turbulent regime based on Nie and Armaly (2004). Note the jump in the Reynolds values at the right side of the x-axis.

The separation point is located at the edge of the step for the sharp case (Le et al., 1997). Downstream the step a recirculation bubble occur, consisting of a counter-clockwise eddy closest to the step, and then a clockwise eddy (Le et al., 1997). Table 3 presents the end of the first counter-clockwise eddy and the clockwise eddy (the reattachment length) when the velocities are averaged from 12-24 hours using five different values on the viscosity and four different resolutions. The end of the reattachment zone is defined as the location where there is a probability of 0.5 that the velocity will be zero in the last 12 hours of the simulation. The reattachment point is found by searching for the shift in sign for the bottom velocities. As Hanjalić and Jakirlić (1998), it is assumed that long-time averaged values can be compared. Using a resolution of 75x50 grid cells (i.e. $\Delta x = 12$m), the length of the first and the second eddy differs considerably from higher resolution simulations, leading to the conclusion that this resolution is not sufficient to represent the flow properly. Table 4 presents reattachment lengths from literature and these reattachment lengths are illustrated in Figure 8 combined with the reattachment lengths from Table 3. The simulations with $Re = 200$ are within the laminar range and correspond to previously published simulations and laboratory experiments (Table 4). The reattachment length varies between 6.0 and 6.9. For the simulations in the transitional regime, the reattachment lengths increase, also in correspondence with previous experiments, and in the turbulent regime the reattachment lengths stabilizes around 7. In the turbulent regime the simulations with a horizontal resolution of 3 m (300x200 grid cells) gives the closest match to the values from the literature. Still, the flow is influenced by the grid size in all the simulations with Reynolds numbers higher than $2{\cdot}10^3$.

The horizontal bottom velocities are presented in Figure 9 using 150x100 grid cells. For Reynolds number of $2{\cdot}10^2$ a stationary eddy is generated downstream the step. The size of the eddy is constant in time. In the transitional and fully turbulent regime several eddies are generated and the reattachment point propagates backward and forward in time as eddies are released from the reattachment zone. The free moving eddies propagate downstream, and eventually out of the domain. In the transitional regime the release time between subsequent eddies are larger than in the fully turbulent regime. As the viscosities are reduced the release time for the eddies are reduced and new eddies are more frequently formed. The discharge of eddies from the reattachment zone generates a saw tooth pattern in Figure 9 b), c), and d), which has also been observed by Le et al. (1997). Le et al. (1997) observed fluctuations in the reattachment length varying between $x/H = 5$ to 8. Barkley et al. (2002) found that

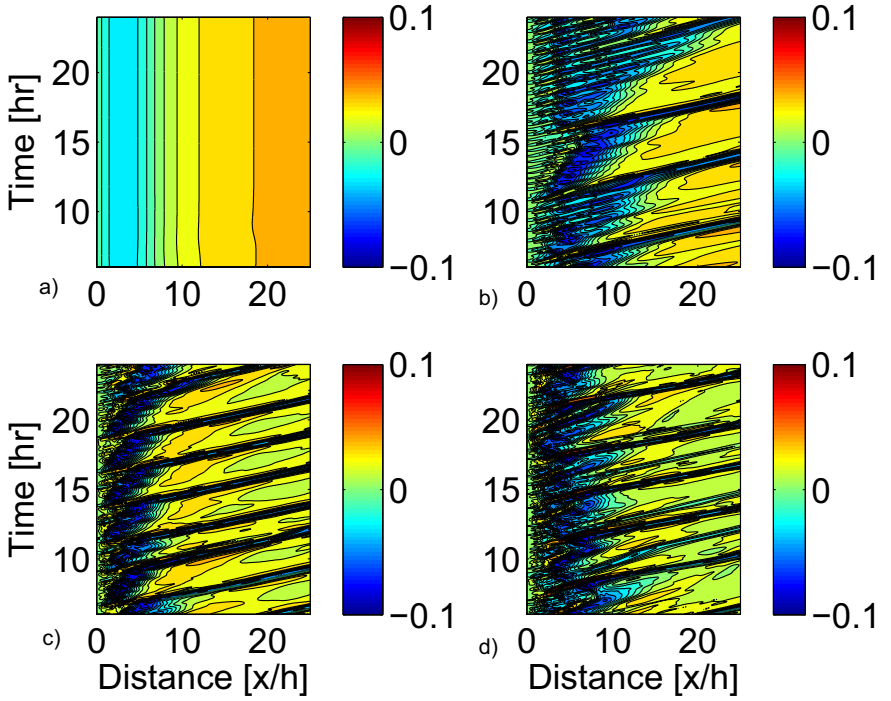

Fig. 9 The horizontal bottom velocities for a) $Re = 2 \cdot 10^2$, b) $Re = 2 \cdot 10^3$, c) $Re = 2 \cdot 10^4$, and d) $Re = 2 \cdot 10^5$ and a resolution of 150x100 grid cells.

flow over a backward facing step was absolute stable up to a Reynolds number of 1050, also in correspondence with the results in this study (Table 4).

References

Adcroft, A., Campin, J.-M., Dutkiewicz, S., Evangelinos, C., Ferreira, D., Forget, G., Fox-Kemper, B., Heimbach, P., Hill, C., Hill, E., Hill, H., Jahn, O., Losch, M., Marshall, J., Maze, G., Menemenlis, D., Molod, A., 2008. MITgcm User Manual. MIT Department of EAPS, 77 Massachusetts Ave, Cambridge, MA 02139-4307.

Adcroft, A., Hill, C., Marshall, J., 1997. Representation of topography by shaved cells in a height coordinate ocean model. Monthly Weather Review, 2293–2315.

Akselvoll, K., Moin, P., 1996. Large eddy simulation of turbulent confined coannular jets and turbulent flow over a backward facing step. Journal of Fluid Dynamics (315), 387–411.

Armaly, B. F., Durst, F., Pereira, J. C. F., Schonung, B., 1983. Experimental and theoretical investigation of backward-facing step flow. Journal of Fluid Mechanics 127, 473–496.

Auerbach, D. I., Caulfield, J. A., Adams, E. E., Herzog, H. J., 1997. Impacts of ocean CO_2 disposal on marine life: I. a toxicological assessment integrating constant-concentration laboratory assay data with variable-concentration field exposure. Environmental Modeling and Assessment 2.

Avlesen, H., Berntsen, J., Espelid, T. O., 2001. A convergence study of two ocean models applied to a density driven flow. International Journal for Numerical Methods in Fluids 36, 639–657.

Bao, F., Dallmann, U. C., 2004. Some physical aspects of separation bubble on a rounded backward-facing step. Aerospace Science and Technology 8, 83–91.

Barkley, D., Gabriela, M., Gomes, M., Henderson, R. D., 2002. Three-dimensional instability in flow over a backward-facing step. Journal of Fluid Mechanics 473, 167–190.

Beaudoin, J.-F., Cadot, O., Aider, J.-L., Wesfreid, J. E., 2004. Three-dimensional stationary flow over a backward-facing step. European Journal of Mechanics B/Fluids 23, 147–155.

Berntsen, J., 2002. Internal pressure errors in sigma-coordinate ocean models. Journal of atmospheric and oceanic technology 19, 1403–1414.

Berntsen, J., 2004. USERS GUIDE for a modesplit σ-coordinate numerical ocean model. Tech. Rep. 4.1, University of Bergen, Johs. Bruns gt. 12, N-5008 BERGEN.

Berntsen, J., Xing, J., Alendal, G., 2006. Assessment of non-hydrostatic ocean models using laboratory scale problems. Continental Shelf Research (26), 1433–1447.

Berntsen, J., Xing, J., Davies, A. M., 2009. Numerical studies of flow over a sill: Sensitivity of the non-hydrostatic effects to the grid size. Ocean Dynamics (59), 1043–1059.

Bravo, H. R., Zheng, Y.-H., 2000. Turbulent flow over step with rounded edges: Experimental and numerical study. Journal of hydraulic engineering, 82–85.

Broecker, W., Peng, T.-H., 1982. Tracers in the sea. Palisades, N.Y.: Lamont-Doherty Geological Observatory, Columbia University.

Chen, Y. T., Nie, J. H., Hsieh, H. T., Sun, L. J., 2006. Three-dimensional convection flow adjacent to inclined backward-facing step. International Journal of Heat and Mass Transfer.

Chiang, T. P., Sheu, T. W. H., 1999. A numerical revisit of backward-facing step flow problem. Physics of Fluids 11 (4), 862–874.

Colling, A., 1989. Ocean circulation, 2nd Edition. The Open University, Walton Hall, Milton Keynes, MK7 6AA, England: Butterworth Heinemann, ISBN: 0 7506 5278 0.

Davies, A. M., Hall, P., 2002. Numerical problems associated with coupling hydrodynamic models in shelf edge regions: the surge event of February 1994. Applied Mathematical Modelling 26, 425–440.

Eaton, J. K., Johnston, J. P., 1981. A review of research on subsonic turbulent flow reattachment. AIAA 19 (9), 1093–1100.

Fer, I., Haugan, P. M., 2003. Dissolution from a liquid CO_2 lake disposed in the deep ocean. Limnology and Oceanography 48 (2), 872–883.

Fessler, J. R., Eaton, J. K., 1999. Turbulence modifiaction by particles in a backward-facing flow. Journal of Fluid Mechanics 394, 97–117.

Fringer, O. B., Gerritsen, M., Street, R. L., 2006. An unstructured-grid, finite-volume, nonhydrostatic, parallel coastal ocean simulator. Ocean Modelling 14, 139–173.

Gartling, D. K., 1990. A test problem for outflow boundary conditions - flow over a backward-facing step. International Journal of Numerical Methods in Fluids 11, 953–967.

Gary, J. M., 1973. Estimation of truncation errors in transformed coordinate, primitive equation atmospheric models. Journal of Atmospheric Science 30, 223–233.

Greenberg, D. A., Dupont, F., Lyard, F. H., Lynch, D. R., Werner, F. E., 2007. Resolution issues in numercal models of oceanic and coastal circulation. Continental Shelf Research 27, 1317–1343.

Hackett, B., Røed, L. P., Gjevik, B., Martinesen, E. A., Eide, L., 1995. A review of the Metocean modeling project (MOMOP) Part 2: Model validation study. Qualitative Skill Assessment for Coastal Ocean Models Coastal and Estuarine Studies 47, 307–327.

Haidvogel, D. B., Beckmann, A., 1998. Numerical Ocean Circulation Modeling. Vol. 2 of Series on Environmental Science and Management. Imperial College Press.

Haney, R. L., 1991. On the pressure gradient force over steep topography in sigma coordinate ocean models. Journal of Physical Oceanography.

Hanjalić, K., Jakirlić, S., 1998. Contribution towards the second-moment closure modelling of separating turbulent flows. Computers & Fluids 27 (2), 137–156.

Haugan, P. M., Alendal, G., 2005. Turbulent diffusion and transport from a CO_2 lake in the deep ocean. Journal of Geophysical Research 110, C09S14.

Hoefener, L., Nitsche, W., 2008. Experimental investigations of controlled transition of a laminar separation bubble in an axisymmetric diffuser. Experimental Fluids 44, 89–103.

House, K. Z., Schrag, D. P., Harvey, C. F., Lackner, K. S., 2006. Permanent carbon dioxide storage in deep-sea sediments. PNAS 103 (33), 12291–12295.

Jovic, S., Driver, D., 1995. Reynolds number effect on the skin friction in separated flows behind a backward-facing step. Experimental Fluids (18), 464–467.

Jovic, S., Driver, D. M., 1994. Backward-facing step measurements at low Reynolds number Re_h=5000. Tech. rep., NASA.

Kaiktsis, L., Karniadakis, G. E., Orszag, S. A., 2006. Unsteadiness and convective instabilities in two-dimensional flow over a backward-facing step. Journal of Fluid Mechanics 321, 157–187.

Kano, Y., Sato, T., Kita, J., Hirabayashi, S., Tabeta, S., 2009. Model prediction on the rise of pCO_2 in uniform flows by leakage of CO_2 purposefully stored under the seabed. International Journal of Greenhouse Gas Control 3, 617–625.

Kantha, L. H., Clayson, C. A., 2000. Small scale processes in geophysical fluid flows. Vol. 67 of International Geophysics Series. Academic Press, ISBN: 0-12-434070-9.

Kantha, L. H., Claysson, C. A., 2000. Numerical models of oceans and oceanic processes. Vol. 66 of International Geophysics Series. Academic Press, ISBN 0-12-434068-7.

Kasagi, N., Matsunaga, A., 1995. Three-dimensional particle-tracking velocimetry measurement of turbulence statistics and energy budget in a backward-facing step flow. International Journal of Heat and Fluid Flow 16, 477–485.

Keilegavlen, E., Berntsen, J., 2009. Non-hydrostatic pressure in σ-coordinate ocean models. Ocean Modelling.

Kim, J., Kline, S. J., Johnston, J. P., 1985. Investigation of a reattaching turbulent shear layer: flow over a backward-facing step. Journal of Fluids Engineering 102, 302–308.

Kundu, P. K., Cohen, I. M., 2004. Fluid Mechanics, 3rd Edition. Elsevier Academic Press, ISBN: 0-12-178253-0.

Le, H., Moin, P., Kim, J., 1997. Direct numerical simulation of turbulent flow over a backward-facing step. Journal of Fluid Dynamics (330), 349–373.

Ledwell, J. R., Watson, A. J., Schmitt, C. S., 1998. Mixing of a tracer in the pycnocline. Journal of Geophysical Research 103 (C10), 21499–21529.

Lee, T., Mateescu, D., 1998. Experimental and numerical investigation of 2-D backward-facing step flow. Journal of Fluids and Structures 12, 703–716.

Lee, Y.-T., Farabee, T. M., Blake, W. K., 2009. Turbulence effects of wall-pressure fluctuations for reattached flow. Computers and Fluids 38, 1033–1041.

Marshall, J., Hill, C., Perelman, L., Adcroft, A., 1997. Hydrostatic, quasi–hydrostatic, and nonhydrostatic ocean modeling. J. Geophys. Res. 102 (C3), 5733–5752.

Martinsen, E. A., Engedahl, H., 1987. Implementation and testing of a lateral boundary scheme as an open boundary condition in a barotropic ocean model. Coastal Engineering (11), 603–627.

McCalpin, J. D., 1994. A comparison of second-order and fourth-order pressure gradient algorithms in a σ-coordinate ocean model. International Journal of Numerical Methods in Fluids 18, 361–383.

Mellor, G. L., Blumberg, A. F., 1985. Modeling vertical and horizontal diffusivities with the sigma coordinate system. Monthly Weather Review 113, 1379–1383.

Mellor, G. L., Oey, L.-Y., Ezer, T., 1998. Sigma coordinate pressure gradient errors and the seamount problem. Journal of Atmospheric and Oceanic Technology 15, 1122–1131.

Neumann, J., Wengle, H., 2003. DNS and LES of passively controlled turbulent backward-facing step flow. Flow, Turbulence and Combustion 71, 297–310.

Neumann, J., Wengle, H., 2004. Coherent structures in controlled separated flow over sharp-edged and rounded steps. Journal of Turbulence 5 (022), 1–24.

Nie, J. H., Armaly, B. F., 2004. Reverse flow regions in three-dimensional backward-facing step flow. International Journal of Heat and Mass Transfer 47, 4713–4720.

Oey, L., Zhang, Y.-H., Chen, P., 1992. Simulation of the Norwegian coastal current in the vicinity of the Halten Bank: Comparison with observations and process study of bank-induced meanders. Journal of Marine Systems 3, 391–416.

Poltzin, K. L., Toole, J. M., Ledwell, J. R., Schmitt, R. W., 1997. Spatial variability of turbulent mixing in the abyssal ocean. Science 276, 93–96.

Rani, H. P., Sheun, T. W. H., Tsai, E. S. F., 2007. Eddy structures in a transitional backward-facing step flow. Journal of Fluid Mechanics 588, 45–58.

Røed, L. P., Hackett, B., Gjevik, B., Eide, L., 1995. A review of the Metocean modeling project (MOMOP), part 1: Model comparison study. Quantitative Skill Assessment for

Coastal Ocean Models Coastal and Estuarine Studies 47, 285–305.
Simpson, R. L., 1996. Aspects of turbulent boundary-layer separation. Progress in Atmospheric Science 32, 457–521.
Smith, J. A., Damm, P. E., Skogen, M. D., Flather, R. A., Pätsch, J., 1996. An investigation into the variability of circulation and transport on the North-West European shelf using three hydrodynamic models. Deutsche Hydrographische Zeitschrift 48, 325–348.
Song, S., DeGraaff, D. B., Eaton, J. K., 2000. Experimental study of a separating, reattaching, and redeveloping flow over a smoothly contoured ramp. International Journal of Heat and Fluid Flow 21, 512–519.
Song, S., Eaton, J. K., 2004. Reynolds number effects on a turbulent boundary layer with separation, reattachment and recovery. Experiments in Fluids (36), 246–258.
Stelling, G. S., van Kester, J. A. T. M., 1994. On the approximation of horizontal gradients in sigma coordinates for bathymetry with steep bottom slopes. International Journal of Numerical Methods in Fluids 18, 915–935.
Thiem, Ø., Berntsen, J., 2006. Internal pressure errors in sigma-coordinate ocean models due to anisotropy. Ocean Modelling 12, 140156.
Thiem, Ø., Berntsen, J., Selvikvåg, K., Fosså, J. H., 2008. Numerical study of particle encounters with an idealized coral reef with focus on grid resolutions and viscosities. BCCS Technical Report Series 24.
Thiem, Ø., Ravagnan, E., Fosså, J. H., Berntsen, J., 2006. Food supply mechanisms for cold-water corals along a continental shelf edge. Journal of Marine Systems 60, 207–219.
Ting, T. S., Prakash, M., Cleary, P. W., Thompson, M. C., 2006. Simulation of high Reynolds number flow over a backward facing step using SPH. ANZIAM J (EMAC2005) 47, C292–C309.
ul Haque, A., Yamada, F. A. S., Chaudhry, S., 2007. Assessment of turbulence models for turbulent flow over backward facing step. Proceedings of the World Congress on Engineering II.
Wasistho, B., Squires, K. D., 2005. Prediction of turbulent separation over a backward-facing smooth ramp. Journal of Turbulence 6 (1).
Williams, P. T., Baker, A. J., 1997. Numerical simulations of laminar flow over a 3D backward-facing step. International Journal for Numerical Methods in Fluids 24, 1159–1183.
Xing, J., Davies, A. M., 2006. Influence of stratification and topography upon internal wave spectra in the region of sills. Geophysical Research Letter.